Journal of Mining and Environment (JME) Vol. 17, No. 1, 2026, 219-238

Shahrood University of Technology

Journal of Mining and Environment (JME)

Journal homepage: www.jme.shahroodut.ac.ir

Iranian Society of Mining Engineering (IRSME)

Assessment of Growth Performance and Biomass Processing of *Odontarrhena inflata* for Nickel Agromining in Serpentine Soils

Saeed Omori1, Arezoo Abedi[1]*, Kumars Seifpanahi-Shabani[1], Hamid Abbasdokht[2], Mohammad Ghafoori[3], Mohammad Abasian[1], Antony van der Ent[4]

1. Department of Mining Engineering, Faculty of Mining, Petroleum & Geophysics Eng, Shahrood University of Technology, Shahrood, Iran
2. Department of Agronomy and Plant Breeding, Faculty of Agriculture, Shahrood University of Technology, Shahrood, Iran
3. Department of Basic Sciences, Shahid Modarres Campus, Farhangian University, Sanandaj, Iran
4. Sustainable Minerals Institute, The University of Queensland, Brisbane, Australia

Article Info

Received 15 July 2025
Received in Revised form 10 August 2025
Accepted 17 August 2025
Published online 17 August 2025

DOI: 10.22044/jme.2025.16509.3230

Keywords

Agromining
Odontarrhena inflata
ANSH
Serpentine soil
Robat-Sefid

Abstract

This study evaluated the efficiency of the native hyperaccumulator Odontarrhena inflata in extracting nickel (Ni) from ultramafic soils in the Robat-Sefid region of northeastern Iran and assessed the feasibility of applying agromining under controlled conditions. A six-month greenhouse experiment was conducted using homogenized serpentine soil with a total Ni concentration of 1,460 mg/kg. By the end of the cultivation period, the aerial parts of the plant yielded 122 g of dry biomass containing 2,195 mg/kg of Ni. The calculated bioconcentration factor (BCF = 1.5) and translocation factor (TF = 3.53) confirmed effective Ni uptake and translocation from roots to shoots. The biomass was pyrolyzed at 550 °C to produce ash, which underwent cross-washing and sulfuric acid (H_2SO_4) leaching. This leaching process achieved a Ni extraction efficiency of 78.9%, and the overall Ni recovery from soil to biomass ash was estimated at 3.53%. Elemental analyses showed substantial reduction of Magnesium (Mg) and Iron (Fe) in the final crystalline product; however, Calcium (Ca) and Sodium (Na) remained at appreciable levels, indicating that further recrystallization or purification steps are necessary to achieve industrial-grade ANSH (ammonium nickel sulfate hexahydrate). Compared with other Ni hyperaccumulators, O. inflata exhibited lower shoot Ni levels than Odontarrhena chalcidica and Alyssum murale, but the combination of its strong ecological adaptability, elevated TF, and native occurrence collectively designates it as a sustainable and promising candidate for agromining applications in nickel-rich soils of Iran.

1. Introduction

Nickel, a critical strategic element in the global mineral economy, plays an indispensable role across numerous industrial and technological sectors due to its exceptional physical and chemical attributes, including superior corrosion resistance, thermal stability, and malleability [4]. Its diverse applications encompass the steel industry, the manufacture of corrosion-resistant alloys, lithium-ion battery cathodes, electroplating processes, and advanced medical technologies [1–3]. In recent years, however, concerns over the security of the global Ni supply have intensified, driven by surging demand—particularly from rapidly expanding renewable energy industries—and the depletion of high-grade ore reserves [5,6]. In response, the development of sustainable methods for Ni recovery from secondary resources such as ultramafic soils, mine waste, electroplating sludge, and electronic waste has become increasingly imperative [7–9]. Such strategies align with the principles of the circular economy and sustainable development, as the valorization of secondary sources not only reduces dependence on primary ores but also mitigates environmental impacts and enhances resource efficiency. Consequently, green technologies such as agromining (agricultural mining) have gained significant attention as viable approaches for sustainable metal recovery,

Corresponding author: abedi.arezoo@gmail.com (A. Abedi)

particularly in regions endowed with low-grade deposits [10,11].

Ultramafic rocks and soils—most notably peridotite and serpentinite—are naturally enriched in metals such as Ni, Cr, and Co. These elements are predominantly hosted in primary minerals, including olivine, pyroxene, and spinel. Through chemical weathering, Ni is released from the silicate lattices of these minerals and subsequently incorporated into secondary phases such as oxides, Fe and Mn hydroxides, or organometallic complexes [12]. Serpentine (ophiolitic) soils, derived primarily from peridotite and serpentinite, cover approximately 1% of the Earth's continental land surface and occur across a wide range of climate zones. These include tropical regions (e.g., New Caledonia, Brazil, Malaysia, Indonesia, Oman) as well as temperate zones (e.g., the United States, several European countries, Australia, Turkey) [13–15]. Characteristically, these soils are rich in heavy metals—particularly Ni, with concentrations typically ranging from 1,700 to 10,000 mg/kg—and contain elevated levels of Mg and Fe, a low calcium-to-magnesium ratio, and deficiencies in essential macronutrients such as nitrogen, phosphorus, and potassium. Such chemical properties impose severe ecological constraints, posing considerable challenges to plant growth and survival [16,17].

Although serpentine soils contain appreciable Ni concentrations, these levels often remain below the economic cutoff for extraction by conventional mining methods. Typically, Ni content ranges from 0.1 to 0.6 wt%, markedly lower than approximately 1.8 wt% found in commercial Ni ores [18–20]. This makes serpentine soils suitable candidates for innovative recovery methods such as phytomining and its advanced variant, agromining. Agromining involves the cultivation of hyperaccumulator plants capable of concentrating target metals in their biomass, which is subsequently harvested, processed thermally, and refined into a metal-rich bio-ore. Conceptualized as an integrated agricultural value chain, the process spans plant cultivation on serpentine substrates to the production of a solid bio-ore enriched with 10–25 wt% of target metals [21]. This approach is typically applied in two contexts: (i) on degraded or abandoned mining sites, and (ii) on agriculturally marginal soils with low productivity, such as serpentine terrain [18,22].

Hyperaccumulator plants are distinguished by their exceptional capacity to absorb, tolerate, and store supraoptimal concentrations of specific metals—including Ni, Zn, Co, and Mg—in their aerial biomass. Typically, these species can accumulate more than 100 mg/kg Cd, 300 mg/kg Co or Cu, 1,000 mg/kg Ni, 3,000 mg/kg Zn, or 10,000 mg/kg Mn in their shoots (on a dry-weight basis) [23,24]. For Ni, the accepted hyperaccumulation threshold exceeds 1,000 mg/kg (on a dry-weight basis). To date, more than 530 nickel-hyperaccumulating species have been identified, with the majority thriving in serpentine ecosystems [25,26]. Notable examples include *Berkheya coddii*, *Alyssum bertolonii*, *Rinorea niccolifera*, and *Odontarrhena muralis*, all recognized for their exceptional efficiency in Ni uptake and accumulation [27–30].

Hyperaccumulator species have been extensively tested in pilot-scale projects targeting Ni recovery from contaminated soils, mine waste, and industrial sludge [31–34]. One of the most prominent global initiatives is the European LIFE-Agromine project, designed to optimize Ni phytorecovery from ultramafic soils in accordance with environmental sustainability and circular economy principles [35]. In Iran, serpentine soils are widespread, offering considerable potential for local agromining ventures [36,37]. Investigations in the ultramafic regions of Kurdistan and Kermanshah provinces have documented serpentine soils with Ni concentrations between 1,030 and 1,470 mg/kg, alongside native nickel-hyperaccumulating plants such as *Odontarrhena inflata*, *Odontarrhena penjwinesis*, and *Odontarrhena callichroa*. These studies have confirmed the strong hyperaccumulation capacity of these species and their promise for agromining applications [38,39]. Additional research has examined the biogeochemistry and metal uptake traits of native flora across various serpentine landscapes in Iran [40–43].

Native to the Mediterranean region, *O. inflata* (family Brassicaceae) is a recognized Ni hyperaccumulator in the serpentine soils of western Iran. This species has demonstrated the ability to store Ni in its aerial biomass at concentrations ranging from 1,105 to 3,700 mg/kg (on a dry-weight basis) [44]. Ammonium nickel sulfate hexahydrate (ANSH) is a high-value compound with wide industrial use, including in chemical manufacturing, electroplating, and catalyst production, and thus commands significant global market interest [45,46].

Despite substantial progress in international agromining research and evidence of nickel-hyperaccumulating species within the ultramafic zones of western Iran, no comprehensive study has yet addressed the growth performance, metal

accumulation efficiency, and Ni recovery potential of *O. inflata* in eastern Iranian serpentine substrates. Given the broad distribution of serpentine formations in eastern Iran, this study aims to address two core questions specific to the Robat-Sefid region: (i) Can *O. inflata* successfully establish and accumulate Ni in the ophiolitic soils of Robat-Sefid? (ii) Is *O. inflata* a viable candidate for Ni agromining under the prevailing environmental and geochemical conditions of the area?

This research presents, for the first time in Iran, an optimized, environmentally sustainable process for Ni recovery from the biomass of the indigenous hyperaccumulator *O. inflata*, culminating in the production of crystalline ANSH. The novelty of this work lies in its systematic integration of biomass washing, acid leaching, and crystallization into a coherent, industrially scalable framework.

2. Materials and Methods

2.1. Geographical Location, Climate, and Geology of the Study Area

The study area, Robat-Sefid, is situated in northeastern Iran at coordinates 35°56′46″N and 59°23′20″E, approximately 65 km south of Mashhad, in Razavi Khorasan Province. Geologically, this region forms part of the Eastern Iran ophiolitic belt and comprises altered ultramafic rocks such as serpentinite, dunite, and harzburgite. Figure 1 presents a satellite image of the study area. The climate of Robat-Sefid is classified as cold semi-arid to arid [47]. Mean annual precipitation ranges from 200 to 300 mm, while the average annual temperature is between 14 and 16°C [48].

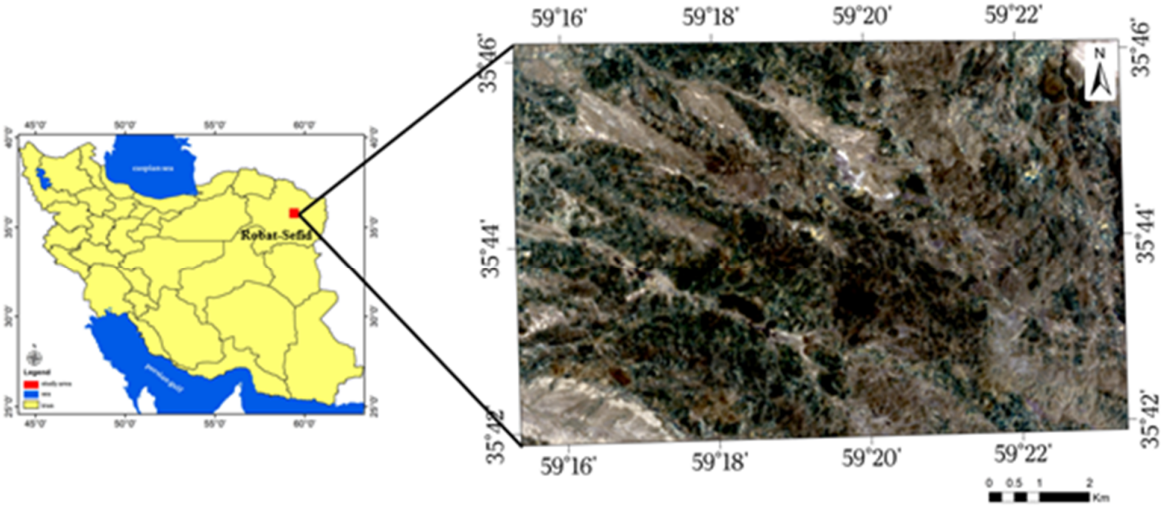

Figure 1. Location of the Robat-Sefid study area in northeastern Iran (Razavi Khorasan Province). The satellite image depicts the distribution of ultramafic units, specifically serpentinized ophiolites (illustrated in green), delineated based on field observations and the 1:100,000 geological map from the Geological Survey of Iran. The

2.2. Soil Collection

In October 2024, a total of 250 kg of soil was collected from the surface horizon (0–20 cm depth) at several sites within the ophiolitic zone of the Robat-Sefid region for use in a greenhouse experiment. The samples were air-dried, passed through a 2-mm sieve, and homogenized to ensure sample uniformity. All processed soils were then thoroughly mixed to produce a single composite sample, which was used as a uniform growth substrate in the experimental pots.

2.3. Plant Species

For this study, *O. inflata* seeds were used for cultivation. These seeds were originally sourced from Kurdistan Province in western Iran. *O. inflata* is a well-documented Ni hyperaccumulator species whose native distribution spans from Iran to Turkmenistan. This species typically thrives in temperate ecosystems [38, 44].

2.4. Experimental Conditions and Design

This study was conducted under semi-controlled greenhouse conditions to evaluate the growth performance and nickel accumulation capacity of *O. inflata* in serpentine soil. The experiment consisted of a single treatment:

cultivation of the plant in serpentine soil collected from the Robat-Sefid region. To ensure uniform environmental conditions and minimize spatial bias, a Completely Randomized Design (CRD) was adopted as the statistical framework.

A total of 21 plastic pots, each with a top diameter of 24 cm, were used as experimental units. Given the substantial influence of soil volume on nickel accumulation in hyperaccumulator species, each pot was filled with 10 kg of homogenized serpentine soil [49]. The pots were randomly arranged on a level greenhouse surface using a random number table to eliminate positional effects. A spacing of 20 cm was maintained between pots in both the horizontal and vertical directions to prevent mutual shading and reduce microclimatic variation.

Initially, *O. inflata* seeds were sown in moist, granular perlite within seedling trays. To enhance germination, the trays were irrigated with deionized water every two days. Following germination, seedlings were grown for three weeks, followed by a four-week acclimation phase during which a diluted nutrient solution (at half strength) was applied. This solution was formulated to mimic the macronutrient composition of serpentine soils [2 mM $MgSO_4$, 1 mM $CaCl_2$, 2 mM KNO_3, and 0.1 mM K_2HPO_4] and optimized for nickel-hyperaccumulating species [50]. This pretreatment was designed to reproduce the low Ca/Mg ratio characteristic of ophiolitic soils and prepare the seedlings for transplantation into native serpentine soil. Prior to transplanting, the soil in each pot was moistened with deionized water until drainage occurred. Five seedlings were initially transplanted into each pot containing 10 kg of soil. Three weeks after transplantation, plant density was standardized by thinning to three seedlings per pot to minimize intrapot competition.

To maintain continuous nutrient availability during the growth period, well-decomposed animal manure was thoroughly incorporated into the potting soil. In addition, plants were regularly fertilized with a balanced NPK solution (20–20–20) prepared with deionized water to supply essential macronutrients [51].

Throughout the cultivation period, all pots were irrigated exclusively with deionized water to avoid the introduction of external elements. Greenhouse temperatures were maintained between 22°C and 27°C, with a photoperiod of 16 hours of light and 8 hours of darkness. The growth cycle lasted 24 weeks, terminating when the plants reached the flowering stage.

2.5. Soil and Plant Characterization

To determine the baseline condition of the soil prior to planting, a composite sample was prepared from the soil used in the pots and subjected to a comprehensive physicochemical analysis. Soil pH was measured by suspending 10 g of air-dried soil in 30 mL of distilled water, followed by measurement with a calibrated pH meter. Electrical conductivity (EC) was determined in the saturated paste extract using an EC meter. Organic matter (OM) content was quantified via the loss-on-ignition (LOI) method, based on weight loss after combustion [52]. Water-holding capacity (WHC) was assessed by adding 50 mL of distilled water to 50 g of dry soil and recording the volume of water retained. Soil texture was determined using the standard hydrometer method.

The cation exchange capacity (CEC) of the soil was determined using the standard saturation method with 1 N ammonium acetate (1 N NH_4OAc) at neutral pH (≈7). In this procedure, ammonium ions first replaced exchangeable cations (Ca^{2+}, Mg^{2+}, K^+, and Na^+) adsorbed onto the surfaces of soil colloids. The adsorbed NH_4^+ ions were then displaced by leaching the soil samples with a 1 N sodium acetate (NaOAc) solution. The concentration of ammonium ions released in the extract was quantified using atomic absorption spectrophotometry (AAS; SOLAAR AA Series, Thermo Elemental, UK).

Total metal concentrations were determined by digesting 0.5 g of dried, powdered soil with aqua regia (a 1:3 mixture of nitric acid and hydrochloric acid), following the protocol described in [53]. The mixture was held at ambient temperature (25°C) for 24 h and subsequently heated on a hot block at approximately 90°C for 2 h. After cooling, the digest was filtered through Whatman No. 40 filter paper and diluted to a final volume of 100 mL with distilled water.

Exchangeable metal concentrations were quantified by mixing 10 g of air-dried, sieved soil with 50 mL of 1 M NH_4NO_3 solution. The suspension was agitated on a magnetic stirrer at 25°C for 2 h, following the method described in [54]. The extract was filtered and transferred into a glass volumetric flask for subsequent analysis. The concentrations of total and exchangeable metals—including Ni, Co, Fe, Mn, Cr, Mg, and Ca—were determined using atomic absorption spectrophotometry (AAS).

At the end of the plant growth period, the harvested plant organs—including leaves, stems, flowers, and roots—were thoroughly rinsed twice

with deionized water to remove any residual soil particles. The cleaned samples were oven-dried at 70°C for 48 h. After recording dry weights, the plant tissues were finely ground, and 0.2 g subsamples from each organ were taken for acid digestion. For this, 2 mL of 30% hydrogen peroxide (H_2O_2) and 3 mL of 65% nitric acid (HNO_3) were added to the samples in 250 mL glass beakers. The mixtures were left at ambient temperature (25°C) for 24 h and then heated on a hot block at 90°C for 2 h. After cooling, the digests were filtered through Whatman No. 40 filter paper and diluted to a final volume of 100 mL with distilled water. Metal concentrations were subsequently measured using atomic absorption spectrophotometry (AAS).

2.6. Plant–Soil Interactions

To assess the plant's Ni accumulation capacity, two key bioconcentration metrics were calculated: the Translocation Factor (TF) and the Bioconcentration Factor (BCF), based on standard equations (1) and (2), as described in [55]. These indices reflect the plant's ability to absorb Ni from the soil and redistribute it within various plant tissues.

$$TF = C_{shoot} / C_{root} \quad (1)$$

$$BCF = C_{shoot} / C_{soil} \quad (2)$$

Where are:
C_{shoot}– Total Ni concentration (mg/kg) in the shoot of the plant (leaf, flower and stem);
C_{root}– Total Ni concentration (mg/kg) in the root;
C_{soil}– Total Ni concentration (mg/kg) in the soil.

2.7. Processing of Ash for Nickel Extraction

To recover Ni from the ash of the hyperaccumulator plant *O. inflata* and to synthesize high-purity ANSH, a multi-step laboratory procedure was developed and implemented [56]. As illustrated in Figure 2, the process comprises biomass preparation, controlled ashing, purification, acid leaching, and crystallization, all contributing to optimized Ni recovery and enhanced product purity.

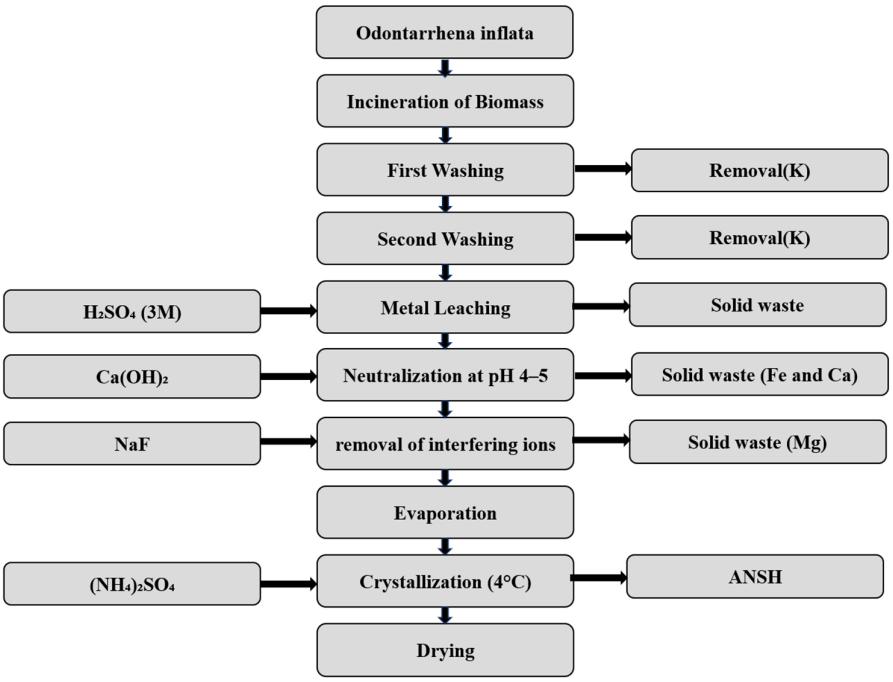

Figure 2. Multistep laboratory process for synthesizing ANSH from the hyperaccumulator plant *Odontarrhena inflata*. Adapted from [56].

2.7.1. Preparation of Plant Biomass

Initially, harvested samples of *O. inflata* were washed with deionized water to remove surface contaminants and dust. The samples were oven-dried at 70°C for 48 h to eliminate residual moisture, ensuring the preservation of metal-bearing mineral structures. The net dry weight of the aboveground biomass (excluding roots) was measured as 122 g and subsequently used for further processing.

2.7.2. Ashing (Pyrolysis)

The dried biomass was ashed in an electric furnace at 550°C for 2 h under oxidative conditions. This temperature was chosen to ensure the complete decomposition of organic matter while preserving metals such as Ni, Fe, and Mg as stable oxides. After cooling in a desiccator, approximately 22.2 g of ash was obtained and designated as bio-ore for the subsequent steps.

2.7.3. Cross-Washing of Ash

To remove soluble salts and alkaline elements such as potassium and sodium, a three-step cross-washing protocol was applied [56]. The ash was split into two equal portions and subjected to three successive washes using 60 mL of deionized water, stirred mechanically at 500 rpm for 10 min at ambient temperature (~25°C). Each filtrate was then used to wash the next portion of ash, enhancing removal efficiency and minimizing water usage. This stage effectively eliminated most soluble impurities [56].

2.7.4. Acid Leaching for Nickel Extraction

The washed ash was subjected to leaching with 3 M sulfuric acid (H_2SO_4) at a solid-to-liquid ratio of 1:10 for 4 h at ambient temperature under continuous magnetic stirring. During this process, Ni, Mg, Ca, and Fe ions were solubilized as their respective sulfates, resulting in the formation of leachate (L1). The primary objective of this step was to selectively extract the target metals from the ash in preparation for downstream separation and purification processes [56].

2.7.5. Neutralization and Removal of Interfering Ions

The L1 leachate was partially neutralized with a 10% (w/w) calcium hydroxide [$Ca(OH)_2$] suspension to adjust the pH to the range of 4.5–5.0. Under these mildly acidic conditions, Fe precipitated as iron hydroxide [$Fe(OH)_3$] and Ca as calcium sulfate ($CaSO_4$), both of which were subsequently removed via filtration. The resulting filtrate (L2) was then treated with a stoichiometric amount of sodium fluoride (NaF), plus an additional 10% excess, to precipitate Mg as magnesium fluoride (MgF_2), yielding the purified solution (L3). This step enhanced the selectivity for Ni by effectively removing interfering ions [56].

Subsequently, L3 was heated at 95°C for 2 h to reduce its volume to one-third, yielding a concentrated solution (L4). This step enhanced Ni ion saturation and created optimal conditions for the crystallization of ANSH. Precise control of temperature and duration was essential to prevent degradation of thermally sensitive components and to maintain product integrity [56].

2.7.6. Crystallization of ANSH

To the concentrated solution (L4), 1 mL of saturated ammonium sulfate [$(NH_4)_2SO_4$] was added to supply NH_4^+ ions required for ANSH crystallization. The resulting solution was stored at 4°C for 24 h in a laboratory refrigerator under controlled slow-cooling conditions to induce supersaturation and facilitate spontaneous crystallization of ANSH. In this step, ammonium sulfate fulfilled multiple roles: supplying ammonium ions, adjusting the pH, and promoting nucleation and growth of the Ni double salt crystals [56].

To evaluate the quality of the ash, intermediate residues, and final crystalline product, a suite of analytical techniques was employed. Elemental composition was assessed using X-ray fluorescence (XRF) spectrometry (Shimadzu XRF-1800). The crystal structure was characterized using Fourier-transform infrared (FTIR) spectroscopy (PerkinElmer Spectrum Two) and Raman spectroscopy (Avantes uRaman-532-Ci). Morphological characteristics were examined using field emission scanning electron microscopy (FESEM). Quantitative results—including Ni recovery efficiency, final product purity, and characterization of by-products—are presented in Sections 3.3 and 3.4. The environmental aspects of the process are discussed in Section 3.5.2.

2.8. Statistical Analysis

Statistical analysis of data obtained from Ni concentration measurements in various plant organs and soil parameters, along with the generation of Raman and FTIR spectra, was performed using OriginPro 2024 and Minitab 19 software. A one-way analysis of variance (ANOVA) was applied to evaluate significant differences among group means, followed by Tukey's post hoc test. All data were presented as mean ± standard deviation (SD), and statistical significance was set at $p < 0.05$.

3. Results and Discussion

3.1. Soil Characteristics

The soil sample exhibited a near-neutral pH of 7.4, favorable for plant growth and within the typical range reported for ultramafic soils (6.1–8.8)

[38, 57–59]. The organic matter (OM) content was relatively low (1.2%), indicating limited potential for nutrient supply via organic compounds. The water-holding capacity (WHC) was 51.6%, and the electrical conductivity (EC) was 537 µS cm^{-1}, suggesting low to moderate salinity. The cation exchange capacity (CEC) was measured at 11.3 cmol kg^{-1}, consistent with the generally low nutrient-retention capacity of ultramafic soils. The soil texture comprised sandy loam, silty loam, and loam, representing a favorable balance between fine and coarse particles that supports both aeration and drainage. The total Ni concentration was 1,460 mg/kg, confirming the metal-rich nature of the soil and aligning with the typical range observed in serpentine terrains (500–8,000 mg/kg) [38, 41, 60] (Table 1).

Table 1. Physicochemical properties of the soil (mean ± standard deviation).

Ni (mg/kg)	pH	OM (%)	WHC (%)	EC ($\mu S\ cm^{-1}$)	CEC (cmol kg^{-1})	Soil Texture
1,460 ± 197	7.4 ± 0.4	1.2 ± 0.3	51.6 ± 4.0	537 ± 17	11.3 ± 0.08	Sandy loam, Silty loam, and Loam

The highest total metal concentration was recorded for Fe (43,068 mg/kg), indicating substantial enrichment. Mg was the second most abundant element (30,294 mg/kg), followed by Ca (11,872 mg/kg), yielding a Ca/Mg ratio of 0.4. This low ratio reflects the dominance of Mg over Ca, a defining characteristic of serpentine soils [38, 61]. The concentrations of other trace metals were as follows: Cr, 769 mg/kg; Mn, 1,345 mg/kg; and Co, 182 mg/kg (Table 2).

Table 2. Total and exchangeable concentrations of selected metals (Mn, Co, Fe, Cr, Ca, and Mg) in the soil (mg/kg), and the Ca/Mg ratio (mean ± standard deviation).

	Mn	Co	Fe	Cr	Ca	Mg	Ca/Mg
Total	1,345 ± 171	182 ± 29	43,068 ± 1,030	769 ± 11	11,872 ± 1,151	30,294 ± 372	0.4 ± 0.04
Exchangeable	0.7 ± 0.5	4.6 ± 3.3	0.9 ± 0.6	33 ± 23.6	3,500 ± 176	12,938 ± 1,347	0.27 ± 0.03

Analysis of the exchangeable metal fractions revealed considerable variation in bioavailability despite the elevated total concentrations of certain elements. For instance, while the total Co concentration was 182 mg/kg, the exchangeable fraction was 4.6 mg/kg—indicating relatively higher bioavailability compared to other heavy metals. Similarly, exchangeable Ca and Mg concentrations were 3,500 mg/kg and 12,938 mg/kg, respectively. Cr displayed a notable exchangeable fraction of 33 mg/kg, suggesting moderate mobility under the prevailing soil chemical conditions. The Ca/Mg ratio in the exchangeable fraction (0.27) was lower than the total Ca/Mg ratio (0.4), reflecting relatively greater Mg bioavailability compared with Ca.

3.2. Plant Characteristics

During the growth period, Ni accumulation in the aerial parts of *O. inflata* was qualitatively assessed using a colorimetric method involving filter paper impregnated with dimethylglyoxime (DMG). The development of a magenta coloration indicated the presence of Ni ions, thereby confirming the plant's capacity for hyperaccumulation [62]. At the flowering stage, after six months of growth, both aerial parts (leaves, flowers, and stems) and roots were harvested for further analysis.

Ni concentrations varied substantially among plant tissues. The shoots exhibited the highest Ni concentration, approximately 2,195 mg/kg, indicating substantial accumulation in the aboveground biomass. In contrast, the roots contained a lower concentration of 621 mg/kg. Additionally, prior to harvesting, the rhizosphere soil exhibited a total Ni concentration of approximately 1,460 mg/kg. These results suggest active uptake of Ni from the soil and efficient translocation from roots to shoots, providing robust evidence for the hyperaccumulation potential of *O. inflata* (Figure 3).

Mg concentrations were measured at 15,700 mg/kg in the shoots and 22,414 mg/kg in the roots of *O. inflata*, indicating a substantial capacity for Mg uptake from serpentine soils. This high level of accumulation highlights the critical physiological roles of Mg in processes such as photosynthesis and enzymatic activity. The Ca/Mg ratio across plant compartments further corroborates this trend, with values of approximately 1.2 in the shoots, 0.2 in the roots, and 0.05 in the rhizosphere—all significantly lower than the ratio observed in the bulk soil (Table 3).

Although the exchangeable Ni concentration in the rhizosphere was relatively low (4.4 mg/kg), its presence indicates sufficient Ni bioavailability in the root zone, potentially contributing to the

observed uptake pattern. Despite the low exchangeable Ni concentration, the plant demonstrated efficient absorption and translocation of Ni, likely facilitated by favorable rhizosphere conditions such as near-neutral pH and moderate cation exchange capacity (CEC). These findings suggest a preferential uptake and accumulation of Mg relative to Ca by *O. inflata*. Notably, Mn and Co were not detected (ND; below the detection limit) in either shoot or root tissues, implying negligible absorption or concentrations below the analytical sensitivity threshold.

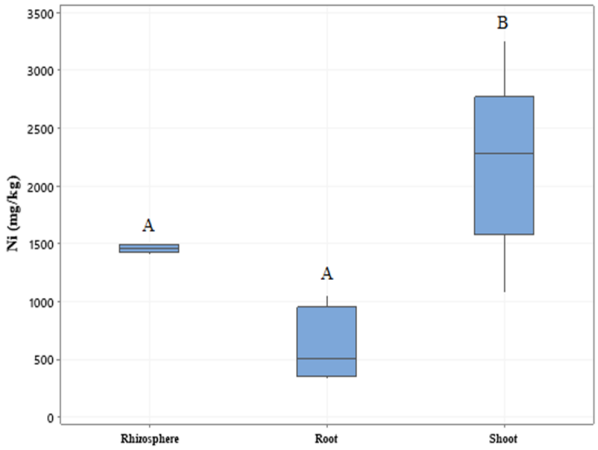

Figure 3. Ni concentrations in the shoots and roots (after six months of growth), as well as in the rhizosphere soil (total Ni content prior to plant harvesting) of *Odontarrhena inflata*. Values represent means (n = 5; biological replicates), and error bars denote the standard error of the mean. Groups not exhibiting statistically significant differences are indicated by identical letters, based on Tukey's multiple comparison test. Letters are assigned within each group analyzed via ANOVA. In each box plot, the central line represents the median, box edges correspond to the first and third quartiles, and whiskers indicate the nonoutlier range.

Table 3. Mean concentrations (± standard deviation) of selected metals (Mn, Co, Fe, Cr, Ca, and Mg) in the shoot, root, and rhizosphere of *Odontarrhena inflata* (mg/kg), and the Ca/Mg ratio.

	Mn	Co	Fe	Cr	Ca	Mg	Ca/Mg
Shoot	ND	ND	1,083 ± 536	392 ± 55	15,477 ± 4,119	15,700 ± 7,785	1.2 ± 0.6
Root	ND	ND	4,034 ± 1,759	407 ± 44	3,464 ± 1,155	22,414 ± 11,659	0.2 ± 0.1
Rhizosphere	1,311 ± 36	66 ± 12	35,275 ± 417	808 ± 9.3	1,676 ± 958	30,147 ± 322	0.05 ± 0.04

ND, not detected

In light of the above results, the bioconcentration factor (BCF) and translocation factor (TF) for Ni were recalculated to improve the accuracy of evaluating *O. inflata's* efficiency in Ni uptake and internal redistribution. Based on the updated measurements and in accordance with Equations (1) and (2), the BCF for Ni in the shoots was determined to be 1.5, indicating that the Ni concentration in the aerial tissues is approximately 50% higher than that in the surrounding soil. This result highlights the plant's substantial ability to extract and accumulate Ni from ultramafic substrates.

Moreover, the TF was calculated to be 3.53, indicating a high efficiency in Ni translocation from roots to shoots. A TF value exceeding 1 is characteristic of hyperaccumulator species and further substantiates the hyperaccumulative behavior of *O. inflata*. After six months of cultivation, a significant decrease in total Ni concentration was observed in the rhizosphere soil (Figure 4), corroborating the species' active role in phytoextraction. Collectively, these findings underscore the exceptional capacity of *O. inflata* to absorb, translocate, and sequester Ni in its aboveground biomass. This performance reinforces its potential as a promising candidate for agromining and phytoremediation in Ni-rich or ultramafic soils. Nevertheless, further field-based studies are warranted to confirm its large-scale effectiveness under natural environmental conditions.

To evaluate the status of *O. inflata* among established Ni hyperaccumulator species, a comparative analysis was performed with several related taxa, primarily within the Brassicaceae family (Table 4). In the present study, the Ni concentration in the aerial biomass of *O. inflata* reached 2,195 mg/kg under greenhouse conditions. Although this value is lower than those reported for prominent species such as *Odontarrhena chalcidica* (16,000 mg/kg), *Alyssum murale*

(11,000 mg/kg), and *Alyssum bertolonii* (7,600 mg/kg), it nonetheless surpasses the recognized hyperaccumulation threshold for Ni (1,000 mg/kg), thereby confirming its suitability for agromining applications.

Differences in accumulation capacity may be attributed to variations in soil characteristics, environmental factors, cultivation practices, or the physiological stage at harvest. Nevertheless, the ability of *O. inflata* to thrive in the ultramafic soils of Iran—combined with its high Ni translocation efficiency (TF > 2) and adaptation to semi-arid climates—positions it as a native, resilient, and promising candidate for the development of sustainable agromining systems at the national scale.

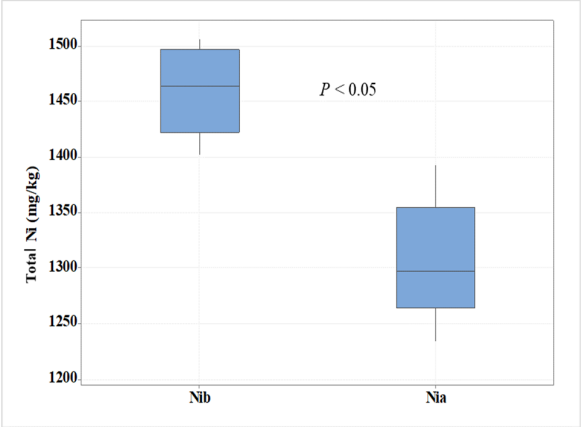

Figure 4. Total Ni concentration in the rhizosphere before (Nib) and after (Nia) the harvesting of *Odontarrhena inflata*. Values represent the mean (n = 5; biological replicates), and error bars indicate the standard error of the mean (SEM). The central line within each box plot denotes the median, while the box edges correspond to the first and third quartiles. Whiskers represent the range of data excluding statistical outliers.

Table 4. Comparative data on Ni concentration and biomass yield in selected hyperaccumulator plant species.

plant species	Family	Ni concentration in biomass (mg/kg)	References
Odontarrhena penjwinensis	Brassicaceae	3,270	[38]
Berkheya coddii	Asteraceae	7,940	[63]
Odontarrhena chalcidica	Brassicaceae	16,000	[63]
Alyssum murale	Brassicaceae	11,000	[64]
Noccaea caerulescens	Brassicaceae	3,627	[7]
Bornmuellea emarginata	Brassicaceae	6,174	[7]
Alyssum bertolonii	Brassicaceae	7,600	[65]
Leptoplax emarginata	Brassicaceae	4,500	[66]

3.3. Nickel Recovery Efficiency from Biomass

At the end of the cultivation period, a total of 122 g of dry biomass was obtained from the aerial parts of *O. inflata*. Following the thermal processing procedures outlined in Section 2.7, this biomass produced 22.2 g of ash (bio-ore), corresponding to an ash yield of 18.2%. X-ray fluorescence (XRF) analysis of the resulting raw ash (RA) revealed a Ni concentration of 1.41 wt% (Table 5). To remove interfering soluble salts such as K_2SO_4, K_2CO_3, and KCl, a three-step cross-washing procedure was conducted using deionized water. This process reduced the total salt content from 17% to 5.25%, while increasing the Ni concentration in the washed ash (WA) to 2.32 wt%, indicating effective impurity removal and enrichment of the target metal. These findings are consistent with previous studies [56, 67–69].

During the leaching process, the washed ash was treated with 3 M sulfuric acid at a solid-to-liquid ratio of 1:10 for 4 h at ambient temperature under continuous magnetic stirring. After filtration, XRF analysis of the residual solid (RL) revealed a remaining Ni content of only 0.49 wt%. Based on the initial Ni concentration of 2.32 wt% in the washed ash (WA), the leaching efficiency was calculated to be 78.9%, indicating that the majority of extractable Ni was successfully transferred into the solution phase (Table 5).

To provide a comprehensive evaluation of Ni recovery efficiency from soil to bio-ore, a comparative mass-balance analysis was conducted. Assuming 10 kg of serpentine soil with a total Ni concentration of 1,460 mg/kg, the total Ni input from the growth substrate was 14.6 g. In contrast, the amount of Ni recovered in the ash was 0.516 g (2.32% of 22.2 g), resulting in an overall recovery efficiency of approximately 3.53% from soil to biomass-derived ash. Although modest, this yield demonstrates the feasibility of bioextraction from low-grade ultramafic substrates.

In addition to Ni, the concentrations of other metals were monitored throughout processing. For instance, the Fe content increased from 1.74% in the raw ash (RA) to 3.59% in the washed ash (WA),

likely reflecting the removal of soluble salts and the relative enrichment of insoluble phases during washing. In the residual solid (RL), however, Fe decreased to 1.25%. This reduction, together with the 10.3% Fe content in the final precipitate (PPT), highlights the need for selective Fe removal to enhance Ni purity. For the alkaline earths, Ca increased from 26.8% (RA) to 30.51% (WA) and then decreased to 20.9% (RL). In contrast, Mg dropped markedly from 11.38% (RA) to 0.81% (RL), indicating effective removal during purification.

Overall, integrating washing, leaching, and selective ion-removal steps resulted in a satisfactory Ni recovery along with efficient impurity reduction. While these results confirm the technical feasibility of recovering Ni as ANSH, achieving industrial-grade purity will still require additional refining steps, including pH adjustment, controlled crystallization, and recrystallization [69]. These findings underscore the effectiveness of biochemical strategies for Ni recovery and provide a basis for the localization and scale-up of agromining technologies in the serpentine soils of Iran.

Table 5. Changes in the concentration of metallic elements during different stages of *Odontarrhena inflata* ash processing (wt%).

	Ni	Mn	Na	Fe	S	Ca	Mg	K
RA	1.41	0.07	0.19	1.74	2.54	26.81	11.38	17.0
WA	2.32	0.12	0.07	3.59	0.44	30.51	9.56	5.25
RL	0.49	0.02	0.01	1.25	20.63	20.9	0.81	1.84
PPT	1.5	0.03	8.67	10.3	13.47	0.52	1.17	1.03

Note: RA = raw ash, **WA** = washed ash, **RL** = residual solid, **PPT** = final precipitate.

3.4. Characteristics of ANSH

3.4.1. FESEM Results

Field emission scanning electron microscopy (FESEM), coupled with energy-dispersive X-ray spectroscopy (EDS), was utilized to characterize the crystal morphology and elemental composition of the final product obtained from the biomass of *O. inflata*.

Elemental mapping revealed a spatially uniform distribution of O, S, and Ca across the crystal surface, while Ni exhibited a heterogeneous, spot-like distribution concentrated in specific regions. Na also showed localized accumulation in certain domains. These patterns are clearly visible in the composite EDS map (Figure 5) as well as in the individual elemental distribution maps (Figure 6). Point spectra confirmed that O, S, and Ca were the predominant elements in the crystalline matrix of the final product. The localized enrichment of Ni suggests its selective incorporation into discrete crystalline regions, most likely in the form of nickel–calcium sulfate phases. These observations support the presence of multiphase structures dominated by Ca and Ni sulfate compounds, and highlight the potential need for further purification through recrystallization.

Comparison of the FESEM images of bio-derived ANSH crystals (Figure 7a) and standard industrial ANSH crystals (Figure 7b) revealed notable differences in crystal morphology and surface organization. The crystals synthesized via the bioprocess exhibited smaller dimensions and reduced uniformity, with more irregular surface features compared to the industrial counterpart. These discrepancies may be attributed to residual mineral and organic impurities, as well as to variations in crystallization conditions inherent to the biogenic route. Nevertheless, the observed morphology remains consistent with the characteristic structure of ANSH.

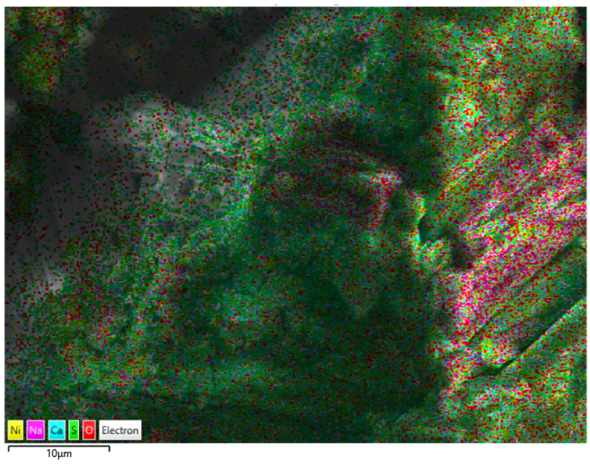

Figure 5. Composite EDS elemental mapping of the final crystalline product derived from *Odontarrhena inflata* biomass, illustrating the spatial distribution of Ni (yellow), S (red), O (green), Na (magenta), and Ca (cyan).

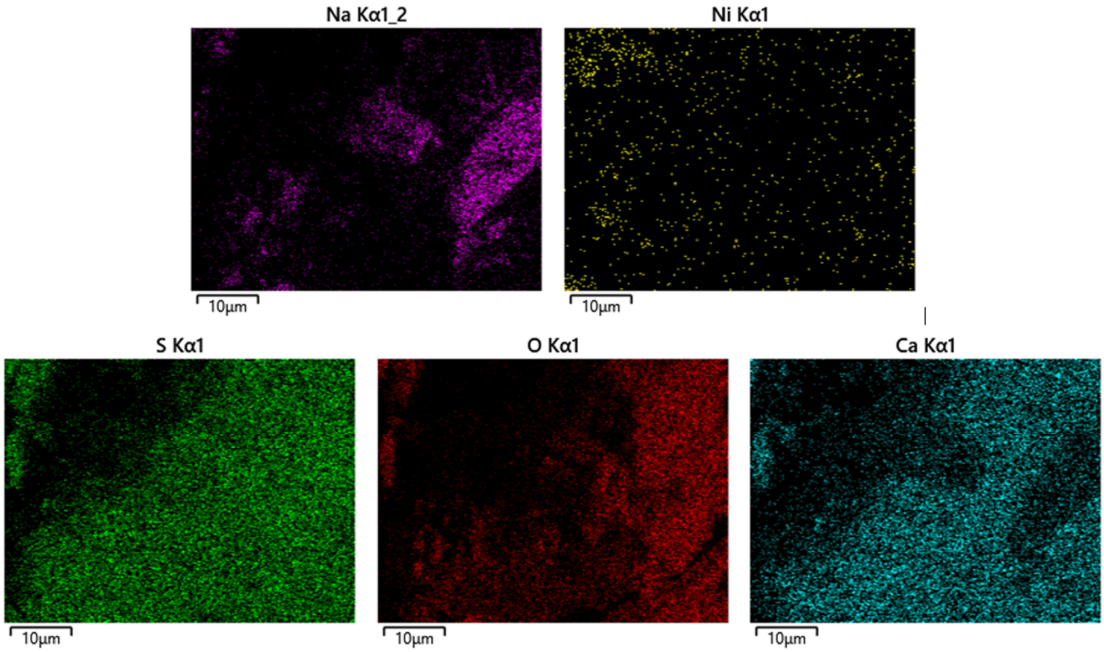

Figure 6. Individual EDS elemental maps of Na, Ni, S, O, and Ca, illustrating their respective spatial distributions across the surface of the crystallized sample.

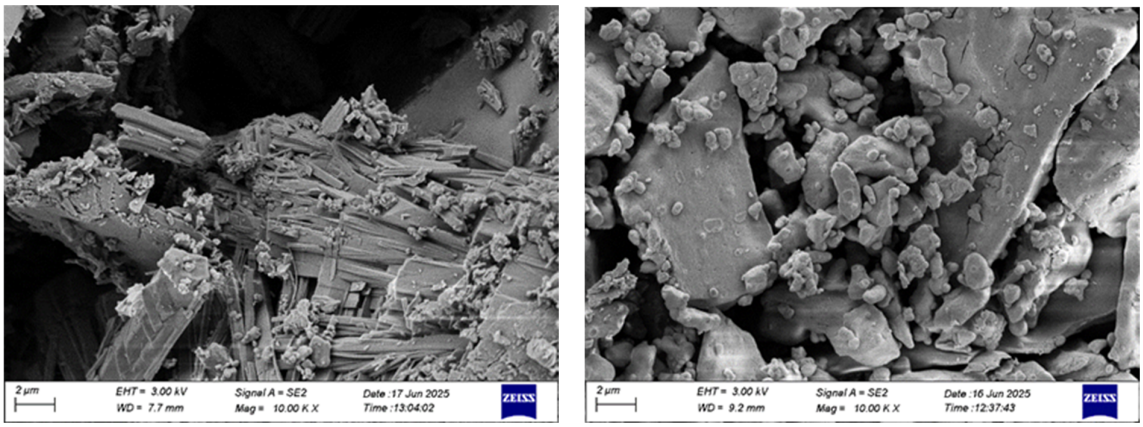

(a)
(b) Reference image of a standard industrial-grade ANSH crystal for structural comparison.

(b)
(a) FESEM image of the ANSH crystal synthesized in this study.

Figure 7. Microscopic and comparative analysis of the final crystalline product. (a) FESEM image of the ANSH crystal synthesized in this study. (b) Reference image of a standard industrial-grade ANSH crystal for structural comparison.

Spot elemental analysis (Table 6) and EDS mapping of the bio-derived ANSH sample identified O, S, Ni, Ca, Na, and trace levels of Mg as the predominant elemental constituents. The corresponding MAP sum spectrum (Figure 8) further corroborated the presence of these elements. As shown in Table 6, O accounted for over 49 wt% on average, highlighting its crucial structural role—likely associated with sulfate groups (SO_4^{2-}) and coordinated water molecules in the hydrated salt. S content ranged from 14.40 wt% (Spectrum 1) to 34.37 wt% (Spectrum 5), consistent with the sulfate-rich nature of the compound. Ni, the target metal, exhibited considerable variation, from 0.29 wt% (Spectrum 2) to 15.76 wt% (Spectrum 3). This heterogeneity likely reflects localized incorporation during crystal growth or competitive substitution by other cations within the crystal lattice.

Ca was detected at concentrations ranging from 8.42 to 35.37 wt%, primarily due to the addition of calcium hydroxide [$Ca(OH)_2$] during the neutralization step of the leach solution. A portion of this Ca was likely incorporated into the crystal

lattice as an impurity. Na, observed at lower concentrations (0.60 to 8.19 wt%), originated from the application of sodium fluoride (NaF) during the Mg removal process. Trace amounts of Mg were also detected in certain regions, likely resulting from residual materials carried over from earlier processing stages.

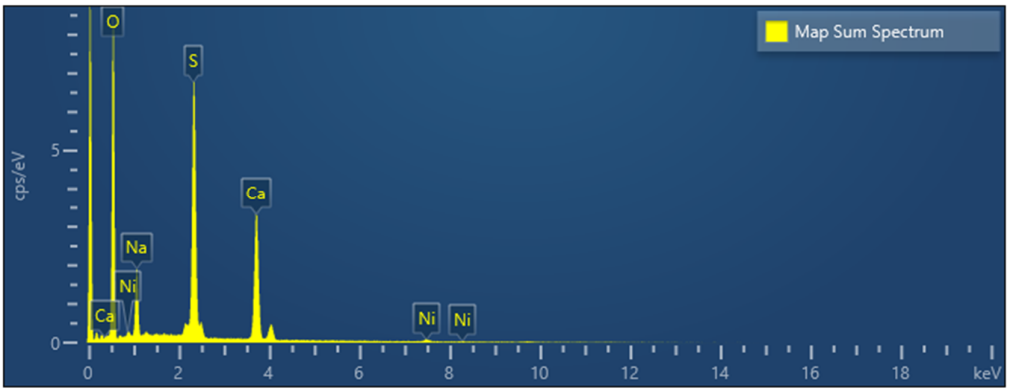

Figure 8. MAP sum spectrum of the ANSH crystal synthesized from *Odontarrhena inflata* biomass, highlighting dominant peaks corresponding to O, S, Ni, Ca, Na, and trace levels of Mg.

Table 6. Elemental composition (wt%) of bio-derived ANSH crystals based on EDS spot analysis (Spectra 1–6).

Spectrum	Spectrum 1	Spectrum 2	Spectrum 3	Spectrum 4	Spectrum 5	Spectrum 6
Ni	0.46 ± 0.19	0.29 ± 0.24	15.76 ± 0.55	11.86 ± 0.82	0.55 ± 0.85	4.80 ± 0.32
S	14.40 ± 0.21	19.56 ± 0.30	24.41 ± 0.35	27.74 ± 0.59	34.37 ± 0.78	25.50 ± 0.29
O	70.92 ± 0.34	59.63 ± 0.50	49.05 ± 0.56	43.79 ± 0.87	28.92 ± 1.21	44.52 ± 0.49
Ca	14.22 ± 0.22	20.52 ± 0.32	9.06 ± 0.22	8.42 ± 0.35	35.37 ± 0.81	24.15 ± 0.30
Na	0	0	1.72 ± 0.14	8.19 ± 0.35	0.79 ± 0.13	0.60 ± 0.08
Mg	0	0	0	0	0	0.43 ± 0.06
Total	100	100	100	100	100	100

Note: All values are reported in weight percent (wt%). A value of "0" indicates that the element was below the detection limit. Spectra were collected from distinct regions of randomly selected ANSH crystals synthesized from *Odontarrhena inflata* biomass.

In contrast, the MAP sum spectrum of the commercial ANSH sample (Figure 9) exhibits pronounced peaks corresponding to O, S, and Ni, with Ca and Na notably absent. This spectral profile indicates the higher purity and structural uniformity of the industrial-grade product. The Ni peak intensities in the commercial sample are significantly greater than those in the biomass-derived counterpart, suggesting more effective incorporation of Ni into the crystal lattice. Moreover, the minimal or absent levels of interfering elements underscore the critical role of recrystallization and advanced purification strategies in producing high-purity ANSH from biogenic sources.

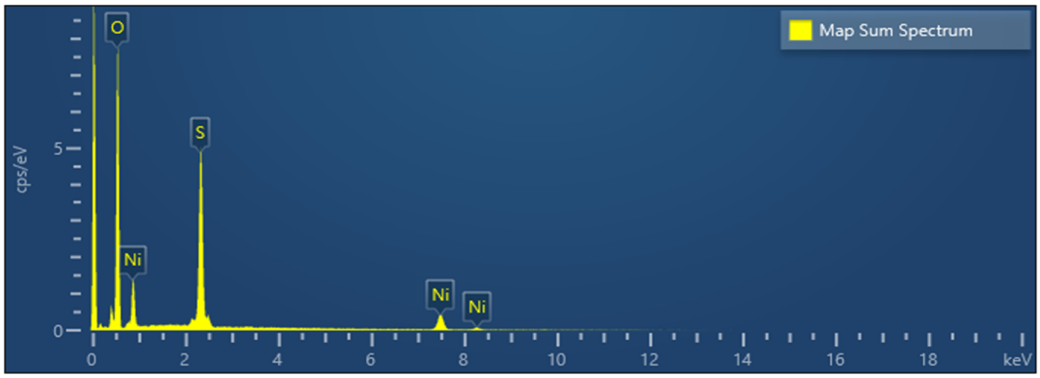

Figure 9. MAP sum spectrum of the standard industrial ANSH crystal (com-ANSH). The spectrum displays prominent peaks corresponding to O, S, and Ni. The absence of Ca and Na signals indicates the superior purity and structural uniformity of the industrial sample compared to the biomass-derived counterpart.

Comparison of the MAP sum spectrum with the elemental data in Table 5 confirms the successful crystallization of ANSH in the biomass-derived product. However, the significant presence of interfering elements such as Ca and Na highlights the need for further recrystallization and purification steps to enhance product purity and meet industrial-grade specifications. Moreover, For the biomass-derived ANSH, the data indicate that O, Ca, and S are the predominant elements in the final crystalline matrix, whereas in the industrial sample Ca is absent.

3.4.2. Raman Spectroscopy Results

Raman spectroscopy was utilized to analyze the molecular structure and vibrational characteristics of synthesized ANSH crystals within the spectral range of 400–3500 cm^{-1}. A comparative analysis between the spectra of the bio-derived sample (bio-ANSH) and the industrial reference (com-ANSH) (Figure 10) revealed several common features along with notable distinctions. In the com-ANSH sample, a sharp and intense peak at approximately 982 cm^{-1} corresponds to the symmetric stretching vibration of the sulfate group (ν_1–SO_4^{2-}), indicating a well-ordered crystalline structure characteristic of ANSH. Furthermore, weaker bands observed at around 627 cm^{-1} and 455 cm^{-1} are assigned to the bending vibrations (ν_4 and ν_2 modes) of the sulfate group, which are consistent with those typically found in hydrated sulfate salts.

In contrast, the Raman spectrum of the bio-derived ANSH (bio-ANSH) exhibited a distinct vibrational profile. A prominent peak around 1000 cm^{-1} is likely attributable to altered symmetry of the sulfate ions or structural disruptions induced by the biosynthesis process. Additionally, a band near 1150 cm^{-1} may indicate the presence of nitrate stretching vibrations or other secondary anionic species, potentially introduced through residual plant metabolites or components of the biological growth medium. A broad band observed near 3400 cm^{-1} corresponds to the stretching vibrations of hydroxyl (O–H) and ammonium (N–H) groups, reflecting the presence of hydration water molecules and ammonium ions within the crystal lattice. Although this band also appears in the com-ANSH spectrum, it is broader and more intense in the bio-derived sample, likely due to organic impurities or variations in the local crystalline environment.

Overall, the Raman spectroscopy results confirmed the formation of a nickel-containing sulfate structure in both samples. However, the spectral differences observed in the bio-ANSH sample reflect the influence of biosynthetic conditions on the molecular configuration and crystalline characteristics of the final product.

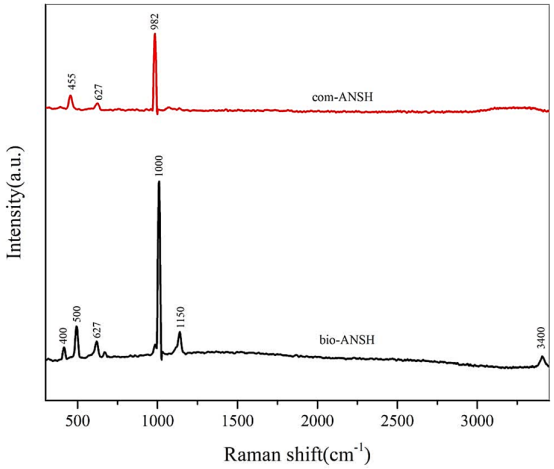

Figure 10. Raman spectra of com-ANSH and bio-ANSH samples. The com-ANSH denotes the industrial-grade standard crystal, whereas bio-ANSH refers to the ANSH product synthesized from biologically processed plant biomass.

3.4.3. FTIR Results

Fourier-transform infrared (FTIR) spectroscopy was utilized to identify functional groups and evaluate the chemical structure of the synthesized ANSH crystals. Comparative analysis of the spectra from the bio-derived sample (bio-ANSH) and the industrial standard (com-ANSH) (Figure 11) confirmed the presence of distinct absorption bands corresponding to sulfate and ammonium functional groups in both specimens.

In the FTIR spectrum of bio-ANSH, a strong absorption band appeared around 1100 cm^{-1}, corresponding to the asymmetric stretching vibration of the sulfate group (ν_3–SO_4^{2-}), indicating the successful incorporation of sulfate units into the crystal lattice. Additionally, a distinct band near 627 cm^{-1} was attributed to the bending vibration (ν_4–SO_4^{2-}) of the sulfate group. A band observed around 1400 cm^{-1} was assigned to the bending vibration of the ammonium group (δ–NH_4^+), confirming the presence of NH_4^+ ions within the ANSH crystal structure.

Furthermore, a broad absorption band in the range of 3200–3400 cm^{-1} was observed, corresponding to the stretching vibrations of hydroxyl (O–H) and ammonium (N–H) groups, indicative of the presence of hydration water molecules and ammonium ions. Additionally, an absorption band near 1640 cm^{-1} was attributed to

the bending vibration of water molecules, further confirming the hydrated nature of the synthesized compound.

Compared to the spectrum of com-ANSH, the bio-ANSH sample exhibited slightly lower intensities and minor shifts in peak positions. These variations may be attributed to residual mineral or organic impurities originating from the bioprocessing steps, as well as differences in synthesis and crystallization conditions. Nevertheless, the overall FTIR spectral profiles of both samples were in strong agreement, confirming the successful formation of crystalline nickel ammonium sulfate hexahydrate in the bio-derived product.

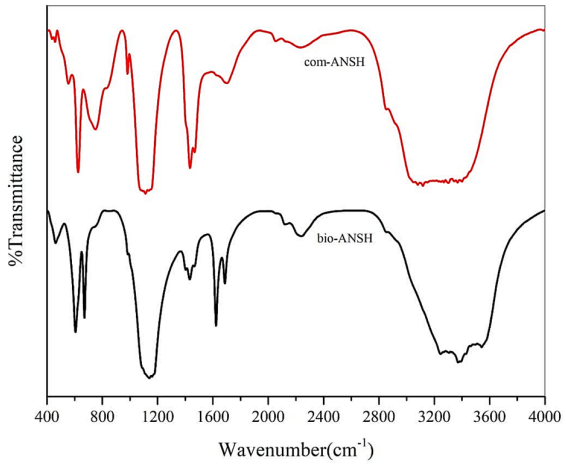

Figure 11. FTIR spectra of com-ANSH and bio-ANSH samples. com-ANSH refers to the industrial standard crystal, while bio-ANSH represents the ANSH crystal obtained through biomass processing.

3.5. Economic and Environmental Assessment

3.5.1. Economic Aspects

Although this study was conducted at laboratory and pilot scales, preliminary evaluations indicate that utilizing the hyperaccumulator plant *O. inflata* for Ni agromining in the serpentine regions of Iran holds considerable economic potential. Experimental data showed that the Ni concentration in the aerial biomass reached 2,195 mg/kg (dry weight). By extrapolating pot-scale results to a per-hectare basis, the estimated annual dry biomass yield under controlled greenhouse conditions was approximately 90–100 kg ha^{-1}. However, this estimate applies specifically to semi-controlled conditions and may vary under open-field cultivation due to environmental and agronomic factors.

While the quantity of Ni recovered at this scale remains limited, the economic outlook improves substantially when the recovered metal is converted into ANSH. This value-added compound possesses greater commercial potential due to its wide-ranging applications in electroplating, chemical synthesis, and catalyst production [45], thereby increasing the overall profitability of the agromining value chain.

Although the process entails substantial operational costs—including harvesting, ashing, chemical reagents, energy consumption, and labor—previous economic assessments of species such as Alyssum murale and *O. chalcidica* have demonstrated that, under favorable conditions and with proper optimization, achieving net profitability is feasible [7, 34]. For example, field trials have reported dry biomass yields of up to 20 t ha^{-1} and Ni concentrations reaching 22 g kg^{-1} in *O. chalcidica*, highlighting the economic viability of large-scale agromining [70]. In South Africa, Ni recovery rates of up to 77 kg ha^{-1} have been reported under optimal conditions using *Berkheya coddii* [71]. Consequently, exporting bio-ore or harvested biomass to countries with advanced Ni extraction technologies could enhance local economic returns and support the production of high-purity Ni sulfate and other value-added products [18].

From an innovation perspective, integrating agromining with advanced techniques such as Enhanced Rock Weathering (ERW) offers a highly promising outlook. In this approach, the application of finely ground silicate minerals—such as basalt—to the soil accelerates chemical weathering processes, promotes atmospheric CO_2 sequestration, enhances micronutrient availability, and ultimately increases metal uptake and accumulation in plants [72–75]. Moreover, because ERW technologies are eligible for carbon credit schemes, their combined implementation with agromining could substantially enhance the economic viability and investment attractiveness of this emerging strategy.

3.5.2. Environmental Aspects

Ni recovery from the biomass of *O. inflata* has been proposed as an innovative and sustainable alternative to conventional extraction methods, offering technically acceptable recovery rates. Nevertheless, it is essential to rigorously assess the potential environmental impacts associated with this process. For example, the ashing step conducted at 550°C may generate gaseous emissions from the combustion of plant-derived organic matter, including CO_2 and volatile organic

compounds (VOCs). The implementation of controlled furnaces and drying systems equipped with advanced filtration technologies can, however, substantially mitigate the release of these pollutants into the atmosphere [76, 77]. Furthermore, integrating agromining with land rehabilitation practices—such as phytoremediation and the reclamation of degraded sites—can improve soil quality, reduce heavy metal contamination, and promote long-term land productivity [18, 78–80].

The adoption of agromining using hyperaccumulator plants such as *O. inflata* represents a novel paradigm for advancing sustainable development within the mining sector. This approach not only aligns with core environmental sustainability principles—by minimizing ecological degradation and reducing reliance on fossil resources—but also enables low-cost, non-invasive metal extraction from nutrient-poor soils. Additionally, coupling this strategy with community-based environmental education initiatives can enhance ecological literacy, reshape public perceptions of mining activities, and foster broader societal engagement in natural resource conservation [81].

Moreover, incorporating agromining into the strategic planning of mining operations—particularly through the use of renewable energy sources during biomass processing and metal recovery stages—can significantly reduce carbon emissions and fossil fuel dependency, thereby contributing to the achievement of long-term sustainability goals [82].

4. Conclusions

The findings of this study clearly indicate that *O. inflata* possesses considerable potential as a Ni hyperaccumulator in the serpentine soils of Iran. Despite the low proportion of exchangeable Ni relative to the total concentration, the low calcium-to-magnesium ratio, and the chemically challenging soil conditions, this species successfully thrived in the native soils of eastern Iran and accumulated substantial amounts of Ni in its tissues.

From an applied perspective, these results present promising opportunities for the deployment of *O. inflata* in agromining initiatives across the ophiolitic regions of Iran, which are predominantly composed of serpentine soils. Moreover, the species demonstrates strong potential for inclusion in phytoremediation programs aimed at rehabilitating nickel-contaminated soils. Cultivation of *O. inflata* on low-productivity or polluted lands could simultaneously facilitate the biological recovery of valuable metals and improve soil quality, thereby contributing to broader environmental restoration efforts. Expanding cultivation to field-scale operations—particularly within Iran's ophiolitic zones can be strategically aligned with national objectives for land rehabilitation and rural development through agromining.

Given that most chromite deposits are associated with serpentinized ultramafic rocks, and considering the large volumes of waste generated from chromite mining and the significant concentrations of Ni present in these tailings [83], future research should investigate the feasibility of Ni recovery from chromite mine tailings using hyperaccumulator plants such as *O. inflata*. This approach could enhance the recovery of valuable metals from secondary resources while aligning with the principles of sustainable development and the circular economy, thereby reducing environmental pollution caused by mining waste.

Nevertheless, the present study was limited to greenhouse and laboratory scales, and several operational challenges—such as field-scale performance, interspecific plant competition under natural conditions, large-scale nutrient management, operational costs, and long-term economic viability—remain to be fully addressed.

In conclusion, this work represents a preliminary yet significant step toward the localization of agromining technology in Iran. Future studies should prioritize: (1) field-scale evaluations of plant performance; (2) optimization of chemical processes to improve the purity of the final product; and (3) comprehensive economic, environmental, and life-cycle assessments to enhance the commercial viability of this technology within the framework of sustainable development.

Acknowledgment

The authors sincerely thank Engineer Fazeli for his invaluable assistance with soil sampling and fieldwork in the study area. His contributions were pivotal to the successful completion of this research.

References

[1]. Kotal, M., Jakhar, S., Roy, S., & Sharma, H. K. (2022). Cathode materials for rechargeable lithium batteries: Recent progress and future prospects. *Journal of Energy Storage*, 47, 103534.

[2] Nickel Institute. (2022). *About nickel*. https://nickelinstitute.org/en/nickel-and-a-low-carbon-future

[3]. Nuhu, B. A., Bamisile, O., Adun, H., Abu, U. O., & Cai, D. (2023). Effects of transition metals for silicon-based lithium-ion battery anodes: A comparative study in electrochemical applications. *Journal of Alloys and Compounds*, 933, 167737.

[4]. U.S. Geological Survey. (2022). *Nickel statistics and information*. https://www.usgs.gov/centers/national-minerals-information-center/nickel-statistics-and-information

[5]. Han, S., Zhenghao, M., Meilin, L., Xiaohui, Y., & Xiaoxue, W. (2023). Global supply sustainability assessment of critical metals for clean energy technology. *Resources Policy*, 85, 103994.

[6]. International Energy Agency. (2025). *Global critical minerals outlook 2025*. https://www.iea.org/reports/global-critical-minerals-outlook-2025

[7]. Cerdeira-Pérez, A., Monterroso, C., Rodríguez-Garrido, B., Machinet, G., Echevarria, G., Prieto-Fernández, Á., & Kidd, P. S. (2019). Implementing nickel phytomining in a serpentine quarry in NW Spain. *Journal of Geochemical Exploration*, 197, 1–13.

[8]. Tognacchini, A., Rosenkranz, T., van der Ent, A., Machinet, G. E., Echevarria, G., & Puschenreiter, M. (2020). Nickel phytomining from industrial wastes: Growing nickel hyperaccumulator plants on galvanic sludges. *Journal of Environmental Management*, 254, 109798.

[9]. Tiseo, I. (2022). *Electric vehicle battery recycling capacity 2021, by country*. Global Tech Environmental. https://www.globaltechenvironmental.com/services/hybrid-ev-battery-recycling

[10]. Junior, A. B. B., Martins, F. P., Cezarino, L. O., Liboni, L. B., Tenório, J. A. S., & Espinosa, D. C. R. (2023). The sustainable development goals, urban mining, and the circular economy. *The Extractive Industries and Society*, 16, 101367.

[11]. Das, A. P., van Hullebusch, E. D., & Akçil, A. (2024). *Sustainable management of mining waste and tailings: a circular economy approach*. CRC Press.

[12]. Kierczak, J., Pietranik, A., & Pędziwiatr, A. (2021). Ultramafic geoecosystems as a natural source of Ni, Cr, and Co to the environment: A review. *Science of the Total Environment*, 755, 142620.

[13]. Galey, M., van der Ent, A., Iqbal, M., & Rajakaruna, N. (2017). Ultramafic geoecology of south and Southeast Asia. *Botanical Studies*, 58(1), 18.

[14]. Hseu, Z.-Y., Zehetner, F., Fujii, K., Watanabe, T., & Nakao, A. (2018). Geochemical fractionation of chromium and nickel in serpentine soil profiles along a temperate to tropical climate gradient. *Geoderma*, 327, 97–106.

[15]. Nascimento, C. W. A. d., Lima, L. H. V., Silva, Y. J. A. B. d., & Biondi, C. M. (2022). Ultramafic soils and nickel phytomining opportunities: A review. *Revista Brasileira de Ciência do Solo*, 46, e0210099.

[16]. Vithanage, M., Kumarathilaka, P., Oze, C., Karunatilake, S., Seneviratne, M., Hseu, Z.-Y., Gunarathne, V., Dassanayake, M., Ok, Y. S., & Rinklebe, J. (2019). Occurrence and cycling of trace elements in ultramafic soils and their impacts on human health: A critical review. *Environment International,* 131, 104974.

[17]. Dushyantha, N., Weerawarnakula, S., Premasiri, R., Abeysinghe, B., Ratnayake, N., Batapola, N., & Ranasinghe, M. (2021). Potential ecological risk assessment of heavy metals (Cr, Ni, and Co) in serpentine soil at Ginigalpelessa in Sri Lanka. *Arabian Journal of Geosciences*, 14(13), 1255.

[18]. van der Ent, A., Baker, A. J., Reeves, R. D., Chaney, R. L., Anderson, C. W., Meech, J. A., Erskine, P. D., Simonnot, M.-O., Vaughan, J., & Morel, J. L. (2015). Agromining: farming for metals in the future? In: ACS Publications.

[19]. Carpen, H. L., & Giese, E. C. (2022). Enhancement of nickel laterite ore bioleaching by Burkholderia sp. using a factorial design. *Applied Water Science*, 12(8), 181.

[20]. Biocyclopedia. (2023). *Nickel.* https://biocyclopedia.com/index/plant_nutrition/essential_elements_micronutrients/nickel/nickel.php

[21]. Morel, J. (2015). Agromining: A new concept. Echevarria G, Morel JL, Simonnot MO, leaders. Workshop,

[22]. Divya, V. U., Sindhu, P. V., & Aiswarya, N. S. (2024). Agromining: Agroremediation for heavy metal contaminated ecosystems: A review. *Bhartiya Krishi Anusandhan Patrika*, 39(1), 51–55.

[23]. Baker, A., & Brooks, R. (1989). Terrestrial higher plants which hyperaccumulate metallic elements. A review of their distribution, ecology and phytochemistry. *Biorecovery*, 1(2), 81–126.

[24]. van der Ent, A., Baker, A., van Balgooy, M., & Tjoa, A. (2013). Ultramafic nickel laterites in Indonesia (Sulawesi, Halmahera): mining, nickel hyperaccumulators and opportunities for phytomining. *Journal of Geochemical Exploration*, 128, 72–79.

[25]. Reeves, R. D., Baker, A. J., Jaffré, T., Erskine, P. D., Echevarria, G., & van der Ent, A. (2018). A global database for plants that hyperaccumulate metal and metalloid trace elements. *New Phytologist*, 218(2), 407–411.

[26]. van der Ent, A., Baker, A. J. M., Echevarria, G., Simonnot, M.-O., & Morel, J. L. (Eds.). (2021).

Agromining: Extracting unconventional resources from plants (2nd ed.; Mineral Resource Reviews). Springer.

[27]. Robinson, B., Brooks, R., Howes, A., Kirkman, J., & Gregg, P. (1997). The potential of the high-biomass nickel hyperaccumulator Berkheya coddii for phytoremediation and phytomining. *Journal of Geochemical Exploration*, 60(2), 115–126.

[28]. Brooks, R., Robinson, B., Howes, A., & Chiarucci, A. (2001). An evaluation of Berkheya coddii Roessler and Alyssum bertolonii Desv. for phytoremediation and phytomining of nickel. *South African Journal of Science*, 97(11), 558–560.

[29]. Leigh Broadhurst, C., Tappero, R. V., Maugel, T. K., Erbe, E. F., Sparks, D. L., & Chaney, R. L. (2009). Interaction of nickel and manganese in accumulation and localization in leaves of the Ni hyperaccumulators Alyssum murale and Alyssum corsicum. *Plant and Soil*, 314(1), 35–48.

[30]. Fernando, E. S., Quimado, M. O., & Doronila, A. I. (2014). Rinorea niccolifera (Violaceae), a new, nickel-hyperaccumulating species from Luzon Island, Philippines. *PhytoKeys*, (37), 1.

[31]. Kidd, P. S., Bani, A., Benizri, E., Gonnelli, C., Hazotte, C., Kisser, J., Konstantinou, M., Kuppens, T., Kyrkas, D., & Laubie, B. (2018). Developing sustainable agromining systems in agricultural ultramafic soils for nickel recovery. *Frontiers in Environmental Science*, 6, 44.

[32]. Rosenkranz, T., Kidd, P., & Puschenreiter, M. (2018). Effect of bacterial inoculants on phytomining of metals from waste incineration bottom ash. *Waste Management*, 73, 351–359.

[33]. Rue, M., Rees, F., Simonnot, M.-O., & Morel, J. L. (2019). Phytoextraction of Ni from a toxic industrial sludge amended with biochar. *Journal of Geochemical Exploration*, 196, 173–181.

[34]. Rosenkranz, T., Hipfinger, C., Ridard, C., & Puschenreiter, M. (2019). A nickel phytomining field trial using Odontarrhena chalcidica and Noccaea goesingensis on an Austrian serpentine soil. *Journal of Environmental Management*, 242, 522–528.

[35]. Echevarria, G. (2015). *LIFE-Agromine project page*. LIFE-Agromine. https://life-agromine.com/en/homepage/

[36]. Moghadam, H. S., Corfu, F., Stern, R. J., & Lotfi Bakhsh, A. (2019). The Eastern Khoy metamorphic complex of NW Iran: a Jurassic ophiolite or continuation of the Sanandaj–Sirjan Zone? *Journal of the Geological Society*, 176(3), 517–529.

[37]. Akbari, S., Karimi, A., Lakzian, A., & Fotovat, A. (2022). Pedogenesis and distribution of Ni and Cr in an ultramafic soil toposequence under arid climate. *Eurasian Soil Science*, 55(4), 520–532.

[38]. Ghafoori, M., Shariati, M., van der Ent, A., & Baker, A. J. (2022). Interpopulation variation in nickel hyperaccumulation and potential for phytomining by Odontarrhena penjwinensis from Western Iran. *Journal of Geochemical Exploration*, 237, 106985.

[39]. Ghafoori, M., Shariati, M., van der Ent, A., & Baker, A. J. (2023). Nickel hyperaccumulation, elemental profiles and agromining potential of three species of Odontarrhena from the ultramafics of Western Iran. *International Journal of Phytoremediation*, 25(3), 381–392.

[40]. Ghaderian, S., & Baker, A. (2007). Geobotanical and biogeochemical reconnaissance of the ultramafics of Central Iran. *Journal of Geochemical Exploration*, 92(1), 34–42.

[41]. Ghaderian, S. M., Mohtadi, A., Rahiminejad, M. R., & Baker, A. J. M. (2007). Nickel and other metal uptake and accumulation by species of Alyssum (Brassicaceae) from the ultramafics of Iran. *Environmental Pollution*, 145(1), 293–298.

[42]. Ghaderian, S. M., Fattahi, H., Khosravi, A. R., & Noghreian, M. (2009). Geobotany and biogeochemistry of serpentine soils of Neyriz, Iran. *Northeastern Naturalist*, 16(sp5), 8–20.

[43]. Mohtadi, A., & Ghaderian, S. M. (2015). Biogeochemistry and geobotany of the serpentine soils of the Rezvanshahr area in northwestern Iran: a preliminary investigation. *Australian Journal of Botany*, 63(4), 367–371.

[44]. Ghaderian, S., Mohtadi, A., Rahiminejad, R., Reeves, R., & Baker, A. (2007). Hyperaccumulation of nickel by two Alyssum species from the serpentine soils of Iran. *Plant and* Soil, 293(1), 91–97.

[45]. Sigma-Aldrich. (2025). *Nickel(II) ammonium sulfate hexahydrate*. https://www.sigmaaldrich.com

[46]. ICIS. (2025). *Nickel ammonium sulfate market insights*. https://www.icis.com

[47]. Najafi, M. S., & Kuchak, V. S. (2024). Ensemble-based monthly to seasonal precipitation forecasting for Iran using a regional weather model. *International Journal of Climatology*, 44(12), 4366–4387.

[48]. Aalijahan, M., & Khosravichenar, A. (2021). A multimethod analysis for average annual precipitation mapping in the Khorasan Razavi Province (Northeastern Iran). *Atmosphere*, 12(5), 592.

[49]. Paul, A. L. D., & Chaney, R. L. (2024). Influence of subsoil and soil volume on the accumulation of nickel by Odontarrhena corsica grown on a serpentine soil. *International Journal of Phytoremediation*, 26(6), 928–935.

[50]. Chaney, R. L., Chen, K.-Y., Li, Y.-M., Angle, J. S., & Baker, A. J. (2008). Effects of calcium on nickel tolerance and accumulation in Alyssum species and

cabbage grown in nutrient solution. *Plant and Soil*, 311(1), 131–140.

[51]. Bani, A., & Echevarria, G. (2019). Can organic amendments replace chemical fertilizers in nickel agromining cropping systems in Albania? *International Journal of Phytoremediation*, 21(1), 43–51.

[52]. Santisteban, J. I., Mediavilla, R., Lopez-Pamo, E., Dabrio, C. J., Zapata, M. B. R., García, M. J. G., Castano, S., & Martínez-Alfaro, P. E. (2004). Loss on ignition: a qualitative or quantitative method for organic matter and carbonate mineral content in sediments? *Journal of Paleolimnology*, 32(3), 287–299.

[53]. Pollard, A. J., McCartha, G. L., Quintela-Sabaris, C., Flynn, T. A., Sobczyk, M. K., & Smith, J. A. C. (2021). Intraspecific variation in nickel tolerance and hyperaccumulation among serpentine and limestone populations of Odontarrhena serpyllifolia (Brassicaceae: Alysseae) from the Iberian Peninsula. *Plants*, 10(4), 800.

[54]. Gryschko, R., Kuhnle, R., Terytze, K., Breuer, J., & Stahr, K. (2005). Soil extraction of readily soluble heavy metals and as with 1 M NH4NO3-solution-evaluation of DIN 19730 (6 pp). *Journal of Soils and Sediments*, 5(2), 101–106.

[55]. Shi, G., & Cai, Q. (2009). Cadmium tolerance and accumulation in eight potential energy crops. *Biotechnology Advances*, 27(5), 555–561.

[56]. Zhang, X., Laubie, B., Houzelot, V., Plasari, E., Echevarria, G., & Simonnot, M.-O. (2016). Increasing purity of ammonium nickel sulfate hexahydrate and production sustainability in a nickel phytomining process. *Chemical Engineering Research and Design*, 106, 26–32.

[57]. Brooks, R. R. (1987). Serpentine and its vegetation. *A multidisciplinary approach*.

[58]. Kruckeberg, A. (1992). Plant life of western North American ultramafics. *In The ecology of areas with serpentinized rocks: a world view* (pp. 31–73). Springer.

[59]. Osmani, M., Bani, A., Gjoka, F., Pavlola, D., Naqellari, P., Shahu, E., Duka, I., & Echevarria, G. (2018). The natural plant colonization of ultramafic post-mining area of Përrenjas, Albania. *Periodico di Mineralogia*, 87, 135–146.

[60]. Nicks, L. J., & Chambers, M. F. (1998). A pioneering study of the potential of phytomining for nickel. *Plants that Hyperaccumulate Heavy Metals: Their Role in Phytoremediation, Microbiology, Archaeology, Mineral Exploration, and Phytomining. CAB International, Wallingford,* UK, 313-325.

[61]. Mizuno, T., & Kirihata, Y. (2015). Elemental composition of plants from the serpentine soil of Sugashima Island, Japan. *Australian Journal of Botany*, 63(4), 252–260.

[62]. Gramlich, A., Moradi, A. B., Robinson, B. H., Kaestner, A., & Schulin, R. (2011). Dimethylglyoxime (DMG) staining for semi-quantitative mapping of Ni in plant tissue. *Environmental and Experimental Botany*, 71(2), 232–240.

[63]. Hipfinger, C., Laux, M., & Puschenreiter, M. (2022). Comparison of four nickel hyperaccumulator species in the temperate climate zone of Central Europe. *Journal of Geochemical Exploration*, 234, 1–10.

[64]. Bani, A., Echevarria, G., Zhang, X., Benizri, E., Laubie, B., Morel, J. L., & Simonnot, M.-O. (2015). The effect of plant density in nickel-phytomining field experiments with Alyssum murale in Albania. *Australian Journal of Botany*, 63(2), 72–77.

[65]. Anderson, C., Brooks, R., Chiarucci, A., LaCoste, C., Leblanc, M., Robinson, B., Simcock, R., & Stewart, R. (1999). Phytomining for nickel, thallium and gold. *Journal of Geochemical Exploration*, 67(1–3), 407–415.

[66]. Pardo, T., Rodríguez-Garrido, B., Saad, R. F., Soto-Vázquez, J. L., Loureiro-Viñas, M., Prieto-Fernández, Á., Echevarria, G., Benizri, E., & Kidd, P. S. (2018). Assessing the agromining potential of Mediterranean nickel-hyperaccumulating plant species at field-scale in ultramafic soils under humid-temperate climate. *Science of the Total Environment*, 630, 275–286.

[67]. Vaughan, J., Riggio, J., Chen, J., Peng, H., Harris, H. H., & van der Ent, A. (2017). Characterisation and hydrometallurgical processing of nickel from tropical agromined bio-ore. *Hydrometallurgy*, 169, 346–355.

[68]. Barbaroux, R., Plasari, E., Mercier, G., Simonnot, M.-O., Morel, J.-L., & Blais, J.-F. (2012). A new process for nickel ammonium disulfate production from ash of the hyperaccumulating plant Alyssum murale. *Science of the Total Environment*, 423, 111–119.

[69]. Marković, B., Jovanović, G., Ranđelović, D., Miletić, M., Vuković, N., Vujović, N., & Sokić, M. (2025). Impact of recrystallization on the purity of ANSH crystals produced from Ni hyperaccumulator Plant. *Tehnika*, 76(1), 45–53.

[70]. Li, Y.-M., Chaney, R. L., Brewer, E. P., Angle, J. S., & Nelkin, J. (2003). Phytoextraction of nickel and cobalt by hyperaccumulator Alyssum species grown on nickel-contaminated soils. *Environmental Science & Technology*, 37(7), 1463–1468.

[71]. Rue, M., Paul, A. L., Echevarria, G., van der Ent, A., Simonnot, M.-O., & Morel, J. L. (2020). Uptake, translocation and accumulation of nickel and cobalt in Berkheya coddii, a 'metal crop' from South Africa. *Metallomics*, 12(8), 1278–1289.

[72]. Vandeginste, V., Lim, C., & Ji, Y. (2024). Exploratory review on environmental aspects of enhanced weathering as a carbon dioxide removal method. *Minerals*, 14(1), 75.

[73]. Bi, B., Li, G., Goll, D. S., Lin, L., Chen, H., Xu, T., Chen, Q., Li, C., Wang, X., & Hao, Z. (2024). Enhanced rock weathering increased soil phosphorus availability and altered root phosphorus-acquisition strategies. *Global Change Biology*, 30(5), e17310.

[74]. Clarkson, M. O., Larkin, C. S., Swoboda, P., Reershemius, T., Suhrhoff, T. J., Maesano, C. N., & Campbell, J. S. (2024). A review of measurement for quantification of carbon dioxide removal by enhanced weathering in soil. *Frontiers in Climate*, 6, 1345224.

[75]. Jerden, J., Mejbel, M., Zamuner Filho, A. N., Carroll, M., & Campe, J. (2024). The impact of geochemical and life-cycle variables on carbon dioxide removal by enhanced rock weathering: Development and application of the Stella ERW model. *Applied Geochemistry*, 167, 106002.

[76]. Tomlinson, S. D., Tsopelakou, A. M., Onn, T. M., Barrett, S. R., Boies, A. M., & Fitzgerald, S. D. (2025). Modelling laminar flow in V-shaped filters integrated with catalyst technologies for atmospheric pollutant removal. *arXiv preprint arXiv*:2506.00603.

[77]. Gahane, D., Biswal, D., & Mandavgane, S. A. (2022). Life cycle assessment of biomass pyrolysis. *BioEnergy Research*, 15(3), 1387–1406.

[78]. Salehi, S., Pouresmaieli, M., & Qarahasanlou, A. N. (2025). A sustainable way to prevent oral diseases caused by heavy metals with phytoremediation. *Case Studies in Chemical and Environmental Engineering*, 11, 101106.

[79] Wang, J., & Delavar, M. A. (2024). Modelling phytoremediation: Concepts, methods, challenges and perspectives. *Soil & Environmental Health*, 2(1), 100062.

[80]. Wang, C., Deng, L., Zhang, Y., Zhao, M., Liang, M., Lee, L.-C., Cristhian, C.-O., Yang, L., & He, T. (2024). Farmland phytoremediation in bibliometric analysis. *Journal of Environmental Management*, 351, 119971.

[81]. Pouresmaieli, M., Ataei, M., Qarahasanlou, A. N., & Barabadi, A. (2024). Building ecological literacy in mining communities: A sustainable development perspective. *Case Studies in Chemical and Environmental Engineering*, 9, 100554.

[82]. Pouresmaieli, M., Ataei, M., Qarahasanlou, A. N., & Barabadi, A. (2023). Integration of renewable energy and sustainable development with strategic planning in the mining industry. *Results in Engineering*, 20, 101412.

[83]. Banerjee, S., Ghosh, S., Jha, S., Kumar, S., Mondal, G., Sarkar, D., Datta, R., Mukherjee, A., & Bhattacharyya, P. (2023). Assessing pollution and health risks from chromite mine tailings contaminated soils in India by employing synergistic statistical approaches. *Science of the Total Environment*, 880, 163228.

نشریه مهندسی معدن و محیط زیست
نشانی نشریه: www.jme.shahroodut.ac.ir
انجمن مهندسی معدن ایران
دانشگاه صنعتی شاهرود

ارزیابی عملکرد رشد و فرآوری زیست‌توده *Odontarrhena inflata* به منظور آگروماینینگ نیکل در خاک‌های سرپانتینی

سعید عموری[۱]، آرزو عابدی[۱*]، کیومرث سیف‌پناهی شعبانی[۱]، محمد غفوری[۲]، محمد عباسیان[۱]، حمید عباسدخت[۳] و آنتونی وان در انت[۴]

۱. گروه مهندسی معدن، دانشکده مهندسی معدن، نفت و ژئوفیزیک، دانشگاه صنعتی شاهرود، شاهرود، ایران
۲. گروه علوم پایه، پردیس شهید مدرس، دانشگاه فرهنگیان، سنندج، ایران
۳. گروه زراعت و اصلاح نباتات، دانشکده کشاورزی، دانشگاه صنعتی شاهرود، شاهرود، ایران
۴. مؤسسه مواد معدنی پایدار، دانشگاه کوئینزلند، بریزبن، استرالیا

اطلاعات مقاله

تاریخ ارسال: ۲۰۲۵/۰۷/۱۵
تاریخ داوری: ۲۰۲۵/۰۸/۱۰
تاریخ پذیرش: ۲۰۲۵/۰۸/۱۷

DOI: 10.22044/jme.2025.16509.3230

کلمات کلیدی

آگروماینینگ
خاک سرپانتینی
Odontarrhena inflata
ANSH
رباط‌سفید

چکیده

این مطالعه کارایی گیاه بومی ابرانباشتگر *Odontarrhena inflata* را در استخراج نیکل (Ni) از خاک‌های اولترامافیک منطقه رباط‌سفید در شمال‌شرق ایران ارزیابی نمود و امکان‌سنجی به‌کارگیری آگروماینینگ در شرایط کنترل‌شده را بررسی کرد. یک آزمایش گلخانه‌ای شش‌ماهه با استفاده از خاک سرپانتینی همگن با غلظت کل نیکل برابر با ۱۴۶۰ میلی‌گرم بر کیلوگرم انجام شد. در پایان دوره کشت، اندام هوایی گیاه ۱۲۲ گرم زیست‌توده خشک با غلظت ۲۱۹۵ میلی‌گرم بر کیلوگرم نیکل تولید کرد. ضریب بیوتراکم (BCF ۱/۵ =) و ضریب انتقال (TF =۳/۵۳) محاسبه‌شده نشان‌دهنده جذب مؤثر نیکل و انتقال آن از ریشه به اندام‌های هوایی بود. زیست‌توده در دمای ۵۵۰ درجه سانتی‌گراد پیرولیز و خاکستر تولید شد که سپس تحت شست‌وشوی متقاطع و لیچینگ با اسید سولفوریک (H_2SO_4) قرار گرفت. این فرآیند لیچینگ بازدهی استخراج نیکل برابر با ۷۸.۹٪ را حاصل کرد و بازیابی کلی نیکل از خاک تا خاکستر زیست‌توده ۳.۵۳٪ برآورد گردید. آنالیزهای عنصری نشان داد که غلظت منیزیم (Mg) و آهن (Fe) در محصول بلوری نهایی به‌طور قابل توجهی کاهش یافت؛ با این حال، مقادیر قابل ملاحظه‌ای کلسیم (Ca) و سدیم (Na) باقی ماند که نشان‌دهنده نیاز به مراحل بازبلورسازی یا خالص‌سازی بیشتر برای دستیابی به ANSH (هگزاهیدرات سولفات نیکل آمونیوم) با درجه صنعتی است. در مقایسه با سایر گیاهان ابرانباشتگر نیکل، *O. inflata* غلظت نیکل کمتری در اندام هوایی نسبت به *Odontarrhena chalcidica* و *Alyssum murale* نشان داد، اما ترکیب ویژگی‌هایی همچون سازگاری اکولوژیکی قوی، ضریب انتقال بالا، و بومی‌بودن این گیاه، آن را به گزینه‌ای پایدار و امیدبخش برای کاربردهای آگروماینینگ در خاک‌های غنی از نیکل ایران تبدیل می‌کند.

نویسنده مسئول مکاتبات: *abedi.arezoo@gmail.com* (آ. عابدی)